Measurement and theoretical modeling of quantum beats in picosecond time-resolved degenerate four-wave mixing and polarization spectroscopy of OH in atmospheric pressure flames

A. A. Suvernev, R. Tadday, and T. Dreier*
Physikalisch Chemisches Institut, Universität Heidelberg, Im Neuenheimer Feld 253, 69120 Heidelberg, Germany
(Received 6 April 1998)

Using tunable ultraviolet picosecond laser pulses pump-probe degenerate four-wave mixing (DFWM) and polarization spectroscopy experiments were conducted in atmospheric pressure flames to investigate the temporal signal behavior in selected rotational transitions of the OH $A\,^2\Sigma - X\,^2\Pi$ (0,0) electronic band. The relaxation behavior of simultaneously excited main and satellite transitions in the Q and P branches was studied in premixed stoichiometric methane-air and hydrogen-oxygen flames. Experimental signal traces are compared with expressions from a detailed theoretical treatment of the signal generation process using perturbation calculations. The theoretical approach consists in calculating the energy density in the signal field mode taking into account the frequency spread of the pump and probe beam radiation, collisional relaxation effects, and the polarization configuration of the incident beams. Relaxation times for population and orientation deduced from the fitting algorithm are in good agreement with DFWM line-shape studies [S. Williams *et al.*, J. Chem. Phys. **104**, 3947 (1996)]. It is shown that quantitative agreement with experimental data obtained for different polarization configurations of pump, probe, and signal photons can be achieved when appropriate time correlated interactions of pump and probe photons are taken into account. In addition, it is shown that due to the frequency spread of the employed laser pulses the different frequency components in the signal beam contribute with different amplitude to the oscillating and nonoscillating parts in the temporal development of the signal intensity depending on the relative strength of the simultaneously excited transitions. [S1050-2947(98)00211-X]

PACS number(s): 42.65.Hw, 42.50.Md, 42.65.An, 42.50.Ct

I. INTRODUCTION

In molecular spectroscopy a common goal of frequency domain experiments is to interpret the relative intensity distributions of the scattered light within a measured optical branch. These are influenced, however, by polarization, relaxation (radiative, energy transfer, quenching), saturation, and dephasing effects. For predictive capabilities of theoretical models these contributions have to be taken into account.

In linear spectroscopic techniques (e.g., spontaneous Raman scattering) a one-to-one correspondence exists between frequency and time-resolved measurements via a Fourier transform [1]. However, in general this relationship breaks down if nonlinear time-resolved spectroscopic techniques are employed. It has been shown that in a given nonlinear optical technique, through proper time sequencing of the interactions of short light pulses with the molecular species certain contributions to the macroscopic polarization responsible for the generated signal intensity can be suppressed [2]. This can lead to a simplification in the interpretation of experiments performed in the time domain. Time-resolved measurements also can reveal interaction induced inherent structures in congested regions of the spectrum, which in the frequency domain may be significantly smoothed due to inhomogeneous broadening. One example is sub-Doppler quantum beat spectroscopy of superposition states excited simultaneously within a single laser pulse [3–5].

In recent years spectroscopic methods that rely on the nonlinear response of the medium have been increasingly used for combustion diagnostics and other gaseous reactive flows [6,7]. These techniques employ the third-order susceptibility resonantly enhanced through atomic or molecular one-photon or multiphoton transitions. Due to their high sensitivity degenerate four-wave mixing (DFWM) [8,9] and polarization spectroscopy (PS) [10,11] are especially attractive among these techniques.

In DFWM, two pump and one probe laser beam of the same frequency intersect in an absorbing medium to generate—via a four-wave-mixing interaction—a fourth beam at the same frequency in a direction determined by phase matching constraints. The DFWM signal generation can be viewed as the Bragg scattering of a probe beam at the volume grating structure formed by the intersecting pump beams that generate a sinusoidal variation of the absorptive or dispersive parts of the complex refractive index of the medium [12,9]. On the other hand, in polarization spectroscopy a strong, linearly or circularly polarized pump beam creates an anisotropy in an absorbing medium that is probed by a weak probe beam of linear polarization. Its depolarization causes light to be observed through a crossed polarizer in the probe beam path. A common feature of both techniques is the generation of a background free signal beam, which can be detected remotely and well isolated from flame luminosity and stray light from a well defined spatial region determined by the interaction volume of the signal generating beams.

Numerous stable and intermediate species important in combustion chemistry, such as OH [13–15], CH [16], C_2H_2 [17], CH_4 [18], NH [19], CN [20], C_2 [21], and NO [22]

*Author to whom correspondence should be addressed. FAX: +49 6221 54 4255. Electronic address: thomas.dreier@urz.uni-heidelberg.de

have been studied using DFWM or PS via electronic or ground-state vibration rotation transitions.

Picosecond time-resolved DFWM/PS experiments have widely been employed for the study of relaxation and dephasing phenomena in small molecules either using absorption [23] or Raman induced [24,25] anisotropies in the medium. Other four-wave-mixing techniques, such as ps-CARS were employed by Akhmanov *et al.* [26] to study rotational relaxation processes at low temperatures in molecular beams of nitrogen seeded in argon.

The relaxation of laser-induced rotational alignment in low pressure samples of NO was experimentally and theoretically analyzed by Schade and co-workers [27]. After picosecond excitation of NO transitions in the $A\,^2\Pi - X\,^2\Sigma$ band the time-resolved laser-induced fluorescence intensity observed with parallel and perpendicular polarization geometry of excitation and detection channels in collisions with CO_2 was investigated. Alignment relaxation times were similar to those measured in our group for OH in atmospheric pressure flames [28,29].

Detailed theoretical models of time-resolved DFWM/PS are scarce or limited to the assumption of cw laser sources, which is quite adequate to describe frequency resolved experiments performed with ns laser pulses. Reichardt *et al.* [30] used direct numerical integration (DNI) of the time dependent density matrix equations to investigate theoretically the use of short pulse lasers in DFWM spectroscopy in gaseous samples. They included Doppler broadening into a two-level model. With parameters most adequate for common experimental conditions—equal pump beam intensities and the probe beam intensity set to one-fourth the peak pump intensity—they calculated for a fixed Doppler width of $\Delta\omega/2\pi c = 0.1\ \mathrm{cm}^{-1}$, a delay of the DFWM signal pulse when the collision rate decreases, whereby the signal pulse length is almost the same as that of the pump pulse. These calculations—although extremely useful for a better understanding of practical measurements—only analyze the delay and shape of the signal pulse relative to the input pulses simultaneously present in the sample. Instead, in the experiments described below the probe is delayed with respect to both pump pulses and the signal pulse is integrated in time, irrespective of its relative delay with respect to the probe pulse.

Using the diagrammatic density-matrix perturbation technique Fujimoto *et al.* have calculated the time evolution of the third-order nonlinear susceptibility for monochromatic external fields [31] and in the case of very short pulses [32]. The theory of DFWM with strong incoherent pump beams has been developed by Cooper *et al.* [33]. Their results describe the steady-state DFWM signal when intense, broad-bandwidth pump lasers interact with a weak monochromatic probe in an optically thin medium composed of two-level atoms. Williams *et al.* [34] developed a perturbative treatment with a spherical tensor analysis to describe DFWM signal intensities taking into account the polarization properties of the molecule-photon interaction. They analyzed DFWM line shapes from selected OH $A\,^2\Sigma - X\,^2\Pi$ (0,0) transitions in atmospheric pressure methane-oxygen flames diluted with helium [35]. Furthermore, Li *et al.* have successfully used this theory to interpret DFWM signal intensities in supersonically cooled pyrazine [36]. These investigations showed that important contributions arise from population, orientation, and alignment in the multipole expansion to the overall DFWM line intensity.

There are several motivations for the present investigation:

(a) In atmospheric pressure flames, besides Doppler and collisional broadening an important part in the contributions to the overall line shape are elastic collisions that reorient the absorbing molecules, i.e., change its orientation and alignment. Therefore, it would be desirable for spectroscopic techniques such as DFWM/PS to determine these individual contributions to the total relaxation rate in different environments in either the frequency or time domain. Williams *et al.* [35] obtained nearly Lorentzian DFWM line profiles for all polarization configurations of the excitation beams for most of their probed transitions, with polarization independent linewidths of $0.043\,\mathrm{cm}^{-1}$. In the present work relaxation times are determined directly from time-resolved picosecond pump-probe DFWM/PS intensity measurements for some OH transitions in atmospheric pressure flames.

(b) It has been suggested that for diagnostic purposes in atmospheric pressure flames the use of picosecond laser pulses in nonlinear optical spectroscopy shortens the interaction time to less than the typical time duration needed for collisional quenching processes to occur, thereby reducing the sensitivity of DFWM/PS to the collision rate.

(c) Finally, of special interest in the present work are simultaneously excited transitions to create superposition states, which can be exploited in high-resolution time-resolved quantum beat spectroscopy [3,4]. For instance, using the two-color laser-induced grating technique with nanosecond laser pulses McCormack *et al.* [5] observed hyperfine quantum beats of NO probed in a molecular beam and demonstrated a spectral resolution almost two orders of magnitude better than the employed laser bandwidths. However, no quantitative theoretical analysis was given to analyze the temporal behavior of the signal traces in different polarization configurations of the excitation and probe beams. A detailed theory would also be beneficial to quantitatively explain recent time-resolved femtosecond four-wave-mixing experiments by Schmitt *et al.* [37] who studied the wave-packet dynamics in the ground and excited states of iodine by CARS and DFWM, respectively.

Recently, we determined relaxation rates within electronic transitions of OH [28] and reported the observation of quantum beats in DFWM and PS experiments in atmospheric pressure flames [29,38]. In the present work these data are analyzed using a perturbative treatment of the time-dependent molecular density matrix. This procedure allowed us to address the various contributions of the transient DFWM/PS signal intensity, and enabled us to determine relaxation times of population and orientation of coherently excited states in the OH $A\,^2\Sigma - X\,^2\Pi$ (0,0) electronic band. It is shown that a detailed modeling of the polarization amplitudes as well as the time ordering in the perturbative treatment of the density operator in nonlinear spectroscopic techniques using short laser pulses are necessary for satisfactory agreement with experiment.

The remaining sections of the paper are organized as follows: Section II gives the theoretical derivation of the time-

resolved DFWM/PS signal intensity. Section III contains a short description of the experimental setup. Sections IV and V present the experimental results together with theoretical modeling and relevant discussions. Finally, concluding remarks are offered in Sec. VI.

II. THEORY

A. General approach

In this section we derive the intensity of the time-dependent four-wave-mixing process. The polarization spectroscopy is treated as a special case of DFWM with copropagating beams. The double interaction of the molecule with the pump beam in a PS experiment is equivalent to interactions with two pump beams in DFWM. Here, the theoretical analysis is conducted using the density matrix formalism. This approach is developed to properly describe relaxation phenomena in the medium. The collisional relaxation processes are treated in this work using a Markovian approximation.

The whole system (radiation+matter) is generally described by the time dependent density matrix $\rho(t)$ [2]. Then, the total energy density of the field mode α existing in the interaction volume V is

$$\varepsilon_\alpha(t)=\frac{\hbar\omega_\alpha}{V}\mathrm{Tr}\{\mathbf{a}_\alpha^\dagger\mathbf{a}_\alpha\rho(t)\}, \tag{1}$$

where $\mathbf{a}_\alpha$ is the annihilation operator and the dagger denotes the Hermitian conjugate (creation) operator. The trace gives the number of photons produced within the interaction volume until time t. A nonequilibrium state of the medium is produced by the preceding pump and probe beams. Furthermore, it is assumed that the external field consists of three laser beams: one probe beam (3) and two pump beams (1, 2). Subsequently, the emission of the signal photons from the probe volume is calculated within the dipole approximation for the interaction between the electric field and the molecules:

$$\mathcal{V}_\alpha=-i\sqrt{\frac{2\pi\hbar\omega_\alpha}{V}}\mathbf{a}_\alpha^\dagger(\mathbf{d}\cdot\mathbf{e}_\alpha^*)\exp(-i\mathbf{k}_\alpha\cdot\mathbf{r}), \tag{2}$$

where $\mathbf{e}_\alpha$ is the polarization unit vector of the field mode α. The dipole moment operator and spatial coordinates of the molecule are denoted by $\mathbf{d}$ and $\mathbf{r}$, respectively. In this work the direction of polarization of the electric field vectors in a laboratory Cartesian frame of reference (X,Y,Z) is denoted from left to right by, e.g., ''$XXYX$,'' for pump beams 1, 2, probe beam 3, and signal beam α, respectively. A circularly polarized field vector is denoted with a ''†'' sign.

The signal emission is described in terms of a second order perturbation expansion in powers of the interaction operator (2). For this purpose we represent the Liouville equation governing the time evolution of the system, in the integral form:

$$\rho(t)=\rho_0-\frac{i}{\hbar}\int_{-\infty}^{t}\exp[-\mathcal{L}(t-t')](\mathcal{V}_\alpha+\mathcal{V}_\alpha^\dagger)^\times\rho(t')dt', \tag{3}$$

where the cross is a shorthand notation for the commutator and $\mathcal{L}$ is the Liouville operator. We further neglect the term ρ_0, which represents the thermal equilibrium (blackbody) radiation. Considering the permutation symmetry of photon operators, one obtains for the total ($t\to\infty$) energy density ($\mathrm{J/m^3}$) emitted from a unit volume:

$$\varepsilon_\alpha=-\sqrt{\pi\hbar}\left(\frac{2\omega_\alpha}{V}\right)^{3/2}\times\mathrm{Re}\int_{-\infty}^{\infty}\mathrm{Tr}\{(\mathbf{d}\cdot\mathbf{e}_\alpha)\exp(i\mathbf{k}_\alpha\cdot\mathbf{r})\mathbf{a}_\alpha\rho(t)\}dt. \tag{4}$$

B. Calculation of the DFWM/PS signal intensity

The signal observed in coherent spectroscopy, such as CARS, DFWM, or PS is produced due to the interaction of each electric field mode with two independent molecules [39,40]. Therefore, expanding Eq. (4) up to second perturbation order we only consider terms relating to such a coherent scattering. In this case, the trace in Eq. (4) in the phase space of the whole system is reduced to the summation over variables of radiation and a single molecule:

$$\mathrm{Tr}\{(\mathbf{d}\cdot\mathbf{e}_\alpha)\exp(i\mathbf{k}_\alpha\cdot\mathbf{r})\mathbf{a}_\alpha\rho(t)\}=-\frac{i}{2\hbar}N(N-1)\mathrm{Tr}_{\mathrm{rad}}\left\{\mathrm{Tr}_1\{(\mathbf{d}\cdot\mathbf{e}_\alpha)e^{i\mathbf{k}_\alpha\cdot\mathbf{r}}\rho_1(t)\}\times\int_{-\infty}^{t}dt'\,\mathrm{Tr}_1\{\mathbf{a}_\alpha e^{-(\mathcal{L}_1+\mathcal{L}_{\mathrm{rad}})(t-t')}\mathcal{V}_\alpha^\times\rho_1(t')\}\rho_{\mathrm{rad}}\right\}, \tag{5}$$

where the subscripts ''1'' and ''rad'' label one-particle and field density matrices, respectively. The classical picture can be used for all incident beams because the number of photons in each of these modes is sufficiently large. Then, the evaluation of the trace in the phase space of radiation is straightforward. Taking into account the conservation of the density-matrix trace in time $[\mathrm{Tr}_1\{\exp(-\mathcal{L}_1t)\mathbf{b}\rho_1\}=\mathrm{Tr}_1\{\mathbf{b}\rho_1\}$, where $\mathbf{b}$ is any molecular operator] one can show that the traces in Eq. (5) lead to complex-conjugate results. Using the following identity for the convolution of complex-conjugate functions

$$2\,\mathrm{Re}\int_{-\infty}^{\infty}f(t)\int_{-\infty}^{t}f^*(t')dt\,dt'=\left|\int_{-\infty}^{\infty}f(t)dt\right|^2 \tag{6}$$

we derive from Eqs. (4) and (5) the desirable expression for the energy density of the coherent signal

$$\varepsilon_\alpha=\pi(n\omega_\alpha)^2\left|\int_{-\infty}^{\infty}\mathrm{Tr}\{(\mathbf{d}\cdot\mathbf{e}_\alpha)\exp(i\mathbf{k}_\alpha\cdot\mathbf{r}-i\omega_\alpha t)\rho(t)\}dt\right|^2, \tag{7}$$

where n is the gas density and the subscript ''1'' is omitted for the sake of simplicity. Note that the density matrix in this expression is modified from the equilibrium distribution due to the interaction of the molecule with the applied electric fields.

C. Calculation of individual interactions of pump-probe photons

The interaction with a relatively weak probe mode can be described by a perturbative approach. Performing the integration in time in Eq. (7) we find

$$\begin{aligned}\int_{-\infty}^{\infty}&\exp(-i\omega_\alpha t)\rho(t)dt\\ &=-\frac{i}{\hbar}\int_{-\infty}^{\infty}\int_{-\infty}^{t}\exp[-i\omega_\alpha t-\mathcal{L}(t-t')]\\ &\quad\times\mathcal{V}(\mathbf{r},t')^{\times}\rho_p(t')dt\,dt'\\ &=-\frac{i}{\hbar}(\mathcal{L}+i\omega_\alpha)^{-1}\int_{-\infty}^{\infty}\exp(-i\omega_\alpha t)\mathcal{V}(\mathbf{r},t)^{\times}\rho_p(t)dt,\end{aligned}\tag{8}$$

where $\mathcal{V}(\mathbf{r},t)=\mathcal{V}_1(\mathbf{r},t)+\mathcal{V}_2(\mathbf{r},t)+\mathcal{V}_3(\mathbf{r},t)$ and $\rho_k(t)$ is the molecular density matrix distorted by the interaction with the pump-probe field mode k. For the incident pulses a Gaussian temporal shape is assumed with dispersion σ. The pump and probe beams are centered at times zero and τ, respectively; e.g., one has for the probe photon:

$$\mathcal{V}_3(t)=E_3\exp[i\omega t-(t-\tau)^2/2\sigma](\mathbf{d}\cdot\mathbf{e}_3^*).\tag{9}$$

The interaction of the molecule with the probe pulse envelope propagating in the direction $\mathbf{n}_3$ is described by the integral

$$\begin{aligned}\mathcal{V}_3(\mathbf{r},t)=\left(\frac{\sigma}{2\pi}\right)^{1/2}&E_3(\mathbf{d}\cdot\mathbf{e}_3^*)\int_{-\infty}^{\infty}\exp[i\omega t-i\mathbf{k}_3(\omega+x)\cdot\mathbf{r}\\ &+ix(t-\tau)-\sigma x^2/2]dx,\end{aligned}\tag{10}$$

where $\mathbf{k}_3(\omega)\approx\mathbf{n}_3\omega/c$ is the wave vector and x denotes a frequency variable. In order to accomplish the time integration in Eq. (8), it is convenient to express $\rho_p(t)$ in terms of the Fourier transform $\tilde{\rho}(x)$ defined as

$$\begin{aligned}\rho_p(t)&=-\frac{i}{\hbar}\int_{-\infty}^{t}\exp[-\mathcal{L}(t-t')]\\ &\quad\times[\mathcal{V}(\mathbf{r},t')+\mathcal{V}^+(\mathbf{r},t')]^{\times}\rho_p(t')dt'\\ &=\int_{-\infty}^{t}dt'\int_{-\infty}^{\infty}dx\exp[-\mathcal{L}(t-t')+ixt']\tilde{\rho}(x).\end{aligned}\tag{11}$$

A simplified solution for $\tilde{\rho}(x)$ is obtained within second order perturbation theory:

$$\begin{aligned}\tilde{\rho}(x)\approx-\frac{1}{2\pi\hbar^2}&\int_{-\infty}^{\infty}dt\,e^{-ixt}[\mathcal{V}(\mathbf{r},t)+\mathcal{V}^+(\mathbf{r},t)]^{\times}\\ &\times\int_{-\infty}^{t}dt'e^{-\mathcal{L}(t-t')}[\mathcal{V}(\mathbf{r},t')+\mathcal{V}^+(\mathbf{r},t')]^{\times}\rho_{\mathrm{eq}},\end{aligned}\tag{12}$$

where ρ_{eq} is the equilibrium density matrix of the molecule.

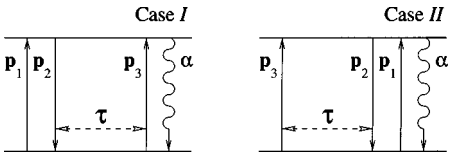

FIG. 1. Energy level diagrams for the time-resolved degenerate four-wave-mixing process. Pump photons are denoted as 1 and 2, the probe photon as 3, and α constitutes the signal photon. Two scattering channels are distinguished: the case where the interaction with the probe wave follows the scattering of both pump photons (case I), and where the probe wave interacts with the molecule before the pump photons (case II). τ is the delay time between pump and probe pulses.

Now, we have to consider the coherent part of Eq. (12), namely, diagrams (e.g., Fig. 1), which provide light scattering in the phase matching direction of the signal beam $\mathbf{k}_\alpha\approx\mathbf{k}_3-\mathbf{k}_2+\mathbf{k}_1$. Note, that the operator $\mathcal{V}(\mathbf{r},t)$ in Eq. (8) describing the last interaction with the applied field is the sum of $\mathcal{V}_3(\mathbf{r},t)$ and $\mathcal{V}_1(\mathbf{r},t)$. These terms determine the signal kinetics at long and short (or negative) delay times (τ). In the following we call them case I and II, respectively. Correspondingly, one has to calculate two separate coherent contributions in Eq. (12):

$$\begin{aligned}\tilde{\rho}(x)_\beta=-\frac{1}{2\pi\hbar^2}&\int_{-\infty}^{\infty}dt\exp(-ixt)\int_{-\infty}^{t}dt'\\ &\times\{\mathcal{V}_\beta(\mathbf{r},t)^{\times}\exp[-\mathcal{L}(t-t')]\mathcal{V}_2^+(\mathbf{r},t')\rho_{\mathrm{eq}}\\ &-\mathcal{V}_2^+(\mathbf{r},t)^{\times}\exp[-\mathcal{L}(t-t')]\rho_{\mathrm{eq}}\mathcal{V}_\beta(\mathbf{r},t')\},\end{aligned}\tag{13}$$

where $\beta=1,3$. Substituting Eqs. (8)–(13) into Eq. (7) and integrating over both time variables we arrive at the following result:

$$\begin{aligned}\varepsilon_\alpha=2\sigma(\pi n\omega_\alpha/\hbar)^2\Bigg|\mathrm{Tr}\Bigg\{&(\mathbf{d}\cdot\mathbf{e}_\alpha)(\mathcal{L}+i\omega_\alpha-i\mathbf{k}_{\boldsymbol{\alpha}}\cdot\mathbf{v})^{-1}\\ &\times\int_{-\infty}^{\infty}dx\exp[-(x+\omega-\omega_\alpha)^2\sigma/2]\times E_3(\mathbf{d}\cdot\mathbf{e}_3^*)^{\times}\\ &\times\exp\{i[\mathbf{k}_\alpha-\mathbf{k}_3(\omega_\alpha-x)]\cdot\mathbf{r}+i(x+\omega-\omega_\alpha)\tau\}\\ &\times(\mathcal{L}+ix)^{-1}\tilde{\rho}_1(x)+E_1(\mathbf{d}\cdot\mathbf{e}_1^*)^{\times}\\ &\times\exp[i(\mathbf{k}_\alpha-\mathbf{k}_1(\omega_\alpha-x)]\cdot\mathbf{r}]\\ &\times(\mathcal{L}+ix)^{-1}\tilde{\rho}_3(x)\Bigg\}\Bigg|^2,\end{aligned}\tag{14}$$

where the permutation property of the Liouville operator: $\exp(i\mathbf{k}_\alpha\cdot\mathbf{r})\mathcal{L}=(\mathcal{L}-i\mathbf{k}_\alpha\cdot\mathbf{v})\exp(i\mathbf{k}_\alpha\cdot\mathbf{r})$ [41] has been employed.

D. Polarization properties of DFWM/PS signal intensity

One of the most important questions for any pump-probe measurements in the gas phase is to find out which relaxation times govern the decay of the signal, i.e., which information about the rotational relaxation process can be extracted from

the measured kinetics. The problem is usually treated in terms of the rotationally irreducible vectors in the Liouville space of the molecule [42]:

$$|i;(f)^{+};K,Q\rangle\rangle=\sum_{m_i,m_f}(-1)^{J_f-m_f}C^{K,Q}_{J_i,m_i;J_f,-m_f}\times|J_i,m_i,k_i\rangle\langle J_f,m_f,k_f|. \quad (15)$$

Here, J and m are the total angular momentum and its projection along a laboratory fixed axis, whereas k labels all other quantum numbers of the selected state. Contrary to the magnetic quantum numbers (m), the rank K of the multipole moment and its projection Q along a laboratory fixed axis are conserved. This is because the relaxation operator has to be invariant with respect to any rotation in the isotropic medium. According to the Wigner-Eckart theorem, the polarization dependence of the dipole operator matrix elements is completely determined by the Clebsch-Gordan coefficients [43]:

$$\langle J',m',k'|(\mathbf{d}\cdot\mathbf{e}_n)|J'',m'',k''\rangle=\sqrt{\frac{\pi\hbar\epsilon_0c^3}{\omega^3_{J'.k';J'',k''}}}A^{1/2}_{J'.k';J'',k''}C^{J',m'}_{J'',m'';1,n}, \quad (16)$$

where $\mathbf{e}_n$ is a spherical basis vector and $A_{J',k';J'',k''}$ is the Einstein coefficient for the transition $J',k'\rightarrow J'',k''$. Expanding $\tilde{\rho}$ in the irreducible basis set (15) we calculate the trace over magnetic quantum numbers in Eq. (14) for the matrix elements (16). The result is represented in the rotationally invariant form where the polarization dependence of the signal intensity is determined by the factors [28]

$$P(\mathbf{e}_1,\mathbf{e}_2;K,Q)=\sum_{n_1,n_2}(-1)^{n_2}(\mathbf{e}^{n_1}\cdot\mathbf{e}_1)(\mathbf{e}^{n_2}\cdot\mathbf{e}_2)^{*}C^{K,Q}_{1,n_1;1,-n_2}. \quad (17)$$

In the Appendix mathematical details can be found describing DFWM signal deconvolution in terms of the multipole moments (15).

E. Time dependence of signal intensity

For arbitrary pulse duration the signal kinetics described by Eqs. (A11), (A13a), and (A13b) is rather complex. However, in the particular case of very short pulses $(\sigma\rightarrow 0)$ the equation is simplified:

$$\varepsilon_\alpha(\tau>0)=\frac{16\pi^4}{k^2}\zeta(T)n^2\sigma^3E_1^2E_2^2E_3^2\left|\sum_{K,Q}P(\mathbf{e}_3,\mathbf{e}_\alpha;K,Q)^{*}P(\mathbf{e}_2,\mathbf{e}_1;K,Q)\sum_{n_1',n_2'}V((\mathcal{L}^{(1)}_{n'',n_2'}+i\omega_\alpha)/kv_T)A_{n_1';n''}A_{n_2';n''}\right.$$
$$\times(2J_1'+1)(2J_2'+1)\left[(-1)^{2J_1'}\exp(-\mathcal{L}^{(K)}_{n_1',n_2'}\tau)\begin{Bmatrix}J'', & J_1', & 1\\ K, & 1, & J_2'\end{Bmatrix}^2\right.$$
$$\left.\left.+(-1)^{J_1'+J_2'}\exp(-\mathcal{L}^{(K)}_{n'',n''}\tau)\begin{Bmatrix}J_1', & J'', & 1\\ K, & 1, & J''\end{Bmatrix}\begin{Bmatrix}J_2', & J'', & 1\\ K, & 1, & J''\end{Bmatrix}\right]\right|^2, \quad (18a)$$

$$\varepsilon_\alpha(\tau<0)=\frac{4\pi^4}{k^2}\zeta(T)n^2\sigma^3E_1^2E_2^2E_3^2\exp[-(kv_T\tau)^2/2]\left|\sum_{K,Q}P(\mathbf{e}_1,\mathbf{e}_\alpha;K,Q)^{*}P(\mathbf{e}_2,\mathbf{e}_3;K,Q)\right.$$
$$\times\sum_{n_1',n_2'}V([\mathcal{L}^{(1)}_{n'',n_2'}+i\omega_\alpha-(kv_T)^2\tau/2]/kv_T)A_{n_1';n''}A_{n_2';n''}$$
$$\times(2J_1'+1)(2J_2'+1)\left[(-1)^{2J_1'}\exp[(\mathcal{L}^{(1)}_{n'',n_2'}+i\omega_\alpha)\tau]\begin{Bmatrix}J'', & J_1', & 1\\ K, & 1, & J_2'\end{Bmatrix}^2\right.$$
$$\left.\left.+(-1)^{J_1'+J_2'}\exp[(\mathcal{L}^{(1)}_{n'',n_1'}+i\omega_\alpha)\tau]\begin{Bmatrix}J_1', & J'', & 1\\ K, & 1, & J''\end{Bmatrix}\begin{Bmatrix}J_2', & J'', & 1\\ K, & 1, & J''\end{Bmatrix}\right]\right|^2, \quad (18b)$$

where $V(x)$ is the complex Voigt function (A7), and $v_T=\sqrt{2k_BT/m}$ is the average thermal velocity of the probed species. It is interesting to mention that the signal behavior at negative delay times (18b) is strictly nonexponential and determined by the thermal distribution over translational velocities. The difference between DFWM at positive and negative delays is illustrated in the scattering diagrams shown in Fig. 1. The density matrix is diagonal (with respect to the main quantum index) after two interactions with the pump photons (case I). The contribution from Doppler motion is canceled if both pump beams are copropagating. This decay of populations is known in the literature as ''T_1 relax-

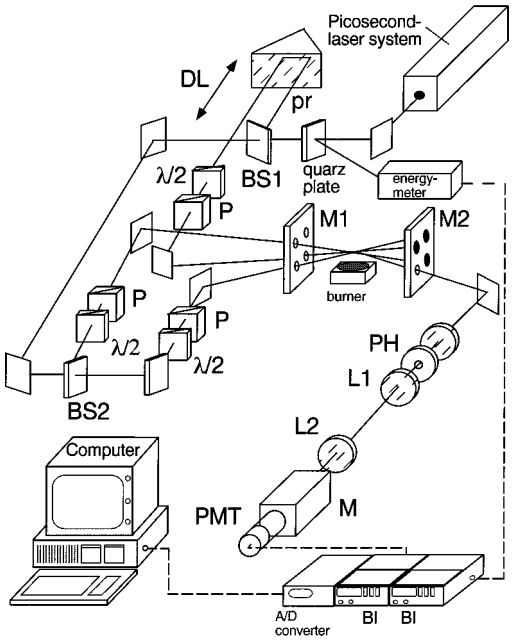

FIG. 2. Experimental setup for pump-probe DFWM in atmospheric pressure flames using a 3D forward folded box beam arrangement. BS1/2, beam splitters; pr, probe beam; DL, optical delay line; P, polarizer; λ/2, half wave plates; M1/2, masks; PMT, photomultiplier; BI, boxcar integrator; M, monochromator; PH, pinhole.

ation'' [44]. In contrast, at negative delays (case II) the τ dependence of the signal is observed after the one-photon interaction of the molecule with the probe wave. In this case the density matrix is off diagonal and the Doppler term is significant. The temporal decay of the off-diagonal density matrix elements is known as phase relaxation, or ''T_2 relaxation'' [44].

III. EXPERIMENT

Using a picosecond laser system time-resolved DFWM and PS signal intensities from selected transitions in the electronic $A\,^2\Sigma - X\,^2\Pi$ (0,0) band system of OH were acquired in one-color pump-probe experiments. Tunable ultraviolet radiation was provided by an amplified and frequency doubled distributed feedback dye laser (DFDL), which was pumped by the second and third harmonic output of a ps Nd:YAG laser. The laser system as well as the experimental PS setup are more fully described in [28,29]. Therefore, in Fig. 2 only the optical arrangement realized in the DFWM experiments is shown schematically. The uv beam around 310 nm was split into two pump beams and one probe beam (pr) by beam splitters BS1,2, and the probe beam was sent through an optical delay line (DL), which consists of a roof prism mounted on a computer controlled translation stage (PI, M-535.22). To avoid saturation effects of the pumped transitions all three beams are combined without focusing into a forward folded box phase matching configuration [34]. The pulse energy in each beam under all conditions was below 1 μJ, which corresponds to less than the calculated spectral saturation intensity of 500 kW/(cm^2 cm^{-1}) for the main Q-branch transitions in the investigated band at 1 atm [45,46]. The alignment of all beams was facilitated by placing two masks with circular holes in the corners of a square at 400 mm on either side from the crossing point above the burner. This arrangement also determined the beam crossing angle of 2.86°, which corresponds to a grating spacing $\Lambda = \lambda/2\sin(\Theta/2) = 6.2$ μm for the excitation beams. The signal beam emerging from the interaction region then passed through the fourth unoccupied corner of one of the masks and was directed through a lens-pinhole (PH, diameter 100 μm) combination onto a photomultiplier (Hamamatsu). The electrical outputs from the photomultiplier and an energy monitor were captured by gated integrators BI (SI, SRS 250) and were further averaged and processed on a PC. The integrators are triggered by a fast photodiode (rise time <1 ns, not shown in Fig. 2), which monitored the 532-nm pulse at the exit of the Nd:YAG pump laser.

The pulse duration was estimated from fitting a sech^2 function to a measured Kerr signal trace obtained in methanol. The frequency distribution of the uv pulse was determined from the spectral intensity distribution in the exit plane of a 0.7-m spectrograph (SPEX, Model 1877) recorded with a charge-coupled-device camera (EG+G, OMAIII) with a spectral resolution of 0.017 nm/pixel. OH radicals were generated in methane-air flames stabilized on a McKenna flat flame burner. Its porous stainless steel plate of 60-mm diameter was kept at 323 K through a cooling water supply. Measurements were done in the center of the flame 6 mm above the burner surface, where a temperature of 2060 $\pm$250 K can be assumed [47]. For the hydrogen-oxygen flames a homemade burner of similar design with a 25-mm diameter brass sinter plate was used, which was supplied with a stoichiometric mixture of 3.6 slm (standard liter per minute) hydrogen and 1.8 slm oxygen. For this mixture a temperature of 1600 K can be estimated [48] 5 mm above the burner surface.

IV. RESULTS

The DFWM and PS signal intensities in Eqs. (A11), (A13a), and (A13b) were calculated numerically using a computer algebra program (MAPLE V). The sums over Q projections of the polarization factors Eq. (17) for ''case I'' in Eq. (A13a) and for ''case II'' in Eq. (A13b) are represented in Table I for different polarization configurations of the input beams. We have summed Eq. (A11) over the frequency spread of the signal photons (ω_α) and varied the center frequency of the spectral intensity distribution within the signal beam for best agreement with experimental data. This variation can be justified because the exact frequency position and spread of the (degenerate) input beams may change from shot to shot and, therefore, was not known during the experiment in which, in addition, several pulses were averaged for each position of the optical delay line. The frequency range to be considered in the modeling is determined by the bandwidth of the incoming beams. Also, the relative strength of the two simultaneously excited transitions determines which part of the spectral intensity distribution of the incoming beams dominates the signal intensity. This situation is schematically illustrated in Fig. 3. In the experiment the center wavelength of the laser beam, as determined with the spectrometer, was chosen to be located between the two closely

TABLE I. Polarization factors $P(\mathbf{e}_1,\mathbf{e}_2;K,Q)$ [from Eq. (17)], which determine the DFWM-PS signal strength as a function of polarization configuration of input and output beams. Subscripts on the polarization unit vector **e** denote the pump beams (1 and 2), probe beam (3), and signal beam (α), respectively. The values for two scattering cases I and II (discussed in the text) are listed separately for each component in the multipole expansion (K) of angular momentum coupling. X,Y,Z denote the polarization along the Cartesian coordinate axis in the laboratory frame, and ''+'' a circularly polarized beam.

Polarization configuration $\mathbf{e}_1\mathbf{e}_2\mathbf{e}_3\mathbf{e}_\alpha$	cf. Fig	Population ($K=0$) I	Population ($K=0$) II	Orientation ($K=1$) I	Orientation ($K=1$) II	Alignment ($K=2$) I	Alignment ($K=2$) II
$XXXX$	6(a)	1/3	1/3	0	0	2/3	2/3
$XXYY$	6(b)	1/3	0	0	1/2	$-1/3$	1/2
$XYYX$	6(c)	0	1/3	1/2	0	1/2	$-1/3$
$XYXY$	6(d)	0	0	$-1/2$	$-1/2$	1/2	1/2
$++XY$	5	0	$-i/6$	$-i/2$	$-i/4$	0	$5i/12$

spaced lines of the main and satellite transition of OH. However, its precise value was not known during the experimental run. In particular, in the simulation of the polarization spectroscopy experiment in the methane-air flame with simultaneous excitation of the $P_2 4$ and $P_{12} 4$ transitions the laser frequency ω was fixed at 32 214.3 cm^{-1}. The corresponding resonance frequencies and Einstein coefficients are given in Table II. In the following, to simulate the experimental PS signal trace the different contributions to the signal intensity of the various frequency components were calculated as a function of the temporal delay between pump and probe photons. As Fig. 4 demonstrates, the signal component at the laser frequency ($\omega_\alpha=\omega$) shows an almost monoexponential decay, whereas the kinetics at frequency components shifted from the laser line center by less than 0.5 cm^{-1} exhibit an oscillatory behavior. As a result, the sum over all signal frequencies contains an observable oscillating contribution above the noise level of the experimental data (crosses in Fig. 5). In this plot, three theoretical curves are shown in addition to the data points of the PS experiment: the solid line is a fit to the experimental data as described above, where only the relative frequency position and width of the incoming beams are varied within experimental uncertainty. The dotted line is a calculation assuming infinitely short laser pulses (delta function in time). This simplification [cf. Eqs. (18a) and (18b)] significantly shortens computation time for calculating the whole signal trace but clearly does not correctly reproduce the experimental data at zero time delay. Finally, the dashed line also results from a simplification of physical assumptions in the theoretical model in that it only considers the intuitively more obvious contribution of case I in the set of important permutations of pump and probe photons in the relevant energy level diagrams depicted in Fig. 1. However, as is obvious from the full simulation the case II interaction of pump and probe photons more properly accounts for the ''negative delay time'' effects at the beginning of the signal trace and has to be included in the simulation.

One of the most interesting features in time-resolved pump-probe DFWM experiments is the strong dependence of the signal kinetics on the polarization geometry of the pump photons, which has been recognized by several authors in frequency-resolved measurements [34–36]. For coherent excitations of transitions with short laser pulses the polarization dependence of the coupling strength of the angular-momentum states of the participating transitions is decisive

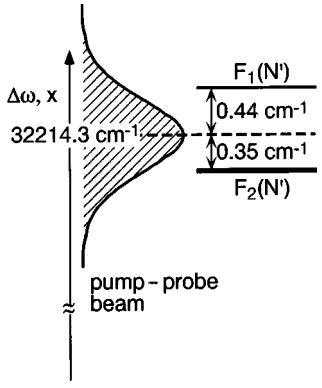

FIG. 3. Schematic representation of upper state OH energy level structure for main and satellite transitions excited in the DFWM/PS experiments ($N'=J'\pm 1/2$). Also shown is the approximate frequency spread and position of the 36-ps excitation pulse.

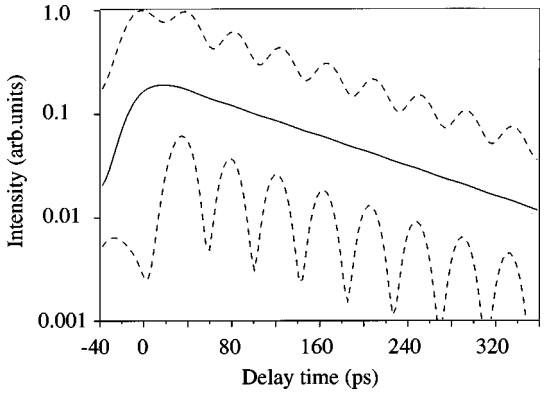

FIG. 4. Calculated time-resolved PS signal intensities for simultaneous excitation of the $P_2 4$ and $P_{12} 4$ transitions of OH with circularly polarized pump pulses. The pulse duration of pump and probe pulses was 36 ps. The solid line is the PS signal at the center frequency of the laser pulse envelope at $\omega_\alpha=32\,214.3$ cm^{-1} (cf., Fig. 3). The dashed curves show, respectively, the signal at the frequency of the $P_{12} 4$ line with $\omega_\alpha=32\,214.74$ (lower curve), and at the frequency of the $P_2 4$ transition with $\omega_\alpha=32\,213.95$ (upper curve). The horizontal axis is the delay time τ between pump and probe pulses.

TABLE II. Transition frequencies and Einstein coefficients for OH in the $A\,^2\Sigma - X\,^2\Pi$ (0,0) electronic band [49] excited in the DFWM/PS experiments. The listed relaxation times are deduced from modeling of the experimental DFWM/PS signal traces. The contributions due to relaxation of population and orientation are listed separately.

Transition	Frequency (cm^{-1})	Einstein coefficient (10^5 s^{-1})	Relaxation times (ps) $1/\Gamma^{(0)}$	$1/\Gamma^{(1)}$	$1/\Gamma^{(2)}$
$P_2 4$	32 213.95	3.822		240	
$P_{12} 4$	32 214.74	1.376		240	
$Q_1 1$	32 474.56	4.104	215	145	
$Q_{21} 1$	32 474.22	5.712	215	145	

for the appearance or nonappearance of quantum beat oscillations in the temporal DFWM intensity profiles. As shown in parts (a) and (b) of Fig. 6, if the polarization vectors of both pump beams are parallel, the decay curve does not show any oscillations caused by the coherent excitation of the two upper molecular levels, at least within the scatter of experimental data taken in the methane-air flame. The respective polarization configuration applied in the experiment is shown as an inset in the upper right corner of each figure. The theoretical trace, however, exhibits some residual oscillatory behavior. This is visible in the full calculations (solid line) as well as in the two limiting cases of infinitely short laser pulses (dotted line) and the case I photon interaction only (dashed line, cf. Fig. 1). On the contrary, in the case of orthogonally polarized pump beams the decay curve exhibits oscillations with a beat frequency corresponding to the splitting of the excited state energy levels [parts (c) and (d) of Fig. 6]. To illustrate the relative importance of the nonoscillating (n) and oscillating (o) contributions to the total signal intensity, we have calculated the maximum amplitudes of these terms in the particular case of infinitely short pulses [Eq. (18a)]. The results are shown as a bar graph in the lower right corner of each figure. Note that the heights of the left bars in each figure are summed up to the vertical size of the graph.

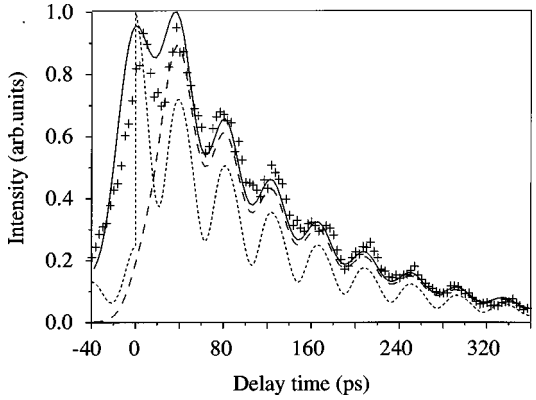

FIG. 5. Experimental PS data (crosses) and model calculation (solid line) for the simultaneous excitation of the $P_2 4$ and $P_{12} 4$ transitions of OH. The calculated kinetics is summed over the entire range of possible signal frequencies (ω_α). The dotted line shows the limiting case of very short pulse lengths given by Eqs. (18a) and (18b). The signal contribution for the case when the probe wave arrives after double interactions of the molecule with the pump beam (case I) is shown by the dashed line. The delay time is given in ps along the x axis.

As one can see from Table I, the DFWM signal intensity in the case of parallel polarized pump beams ($XXXX$ and $XXYY$) contains a nonvanishing isotropic part ($K=0$). The isotropic term provides a dominant contribution, which is determined by values of the 6-j symbols in Eqs. (A13a) and (A13b). Specifically, for the $Q_1 1$ line ($J''=J_1'=J_2'=1$) we have

$$\begin{Bmatrix} 1, & 1, & 1 \\ K=0, & 1, & 1 \end{Bmatrix}^2 \approx 0.1,$$

$$\begin{Bmatrix} 1, & 1, & 1 \\ K=1, & 1, & 1 \end{Bmatrix}^2 = \begin{Bmatrix} 1, & 1, & 1 \\ K=2, & 1, & 1 \end{Bmatrix}^2 \approx 0.028. \quad (19)$$

On the other hand, the oscillating part is forbidden for pure population gratings ($K=0$), because the two excited molecular states have different total angular momentum, and one obtains

$$\begin{Bmatrix} J'', & J_1', & 1 \\ K=0, & 1, & J_2' \end{Bmatrix} \propto \delta_{J_1', J_2'}. \quad (20)$$

Therefore, it turns out that the oscillating term is much smaller relative to the nonoscillating contribution if the polarization vectors of both pump beams are parallel. When the polarization vectors of the electric fields are orthogonal the isotropic term is forbidden (see Table I), and the relative contribution of the oscillating term to the total signal intensity becomes much more important. This is obvious in Fig. 6.

V. DISCUSSION

In time-resolved pump-probe techniques for combustion diagnostics picosecond laser pulses constitute a compromise between sufficient spectral and temporal resolution: characteristic vibronic spectra of many small radicals important in flame chemistry exhibit open spectral regions which allow the excitation of single transitions with coherent radiation of modest bandwidth (0.5–2 cm^{-1}). These pulse characteristics can be achieved with transform limited ps laser pulses in the uv, which simultaneously are sufficiently short to probe relaxation and quenching processes at atmospheric pressure.

From the theoretical derivations and the experimental findings (cf. Fig. 6) it has been shown that in the weak-field limit the signal intensity in time-resolved DFWM/PS is dependent on the spatial anisotropy of the total angular momentum distribution induced by the input fields, which turns

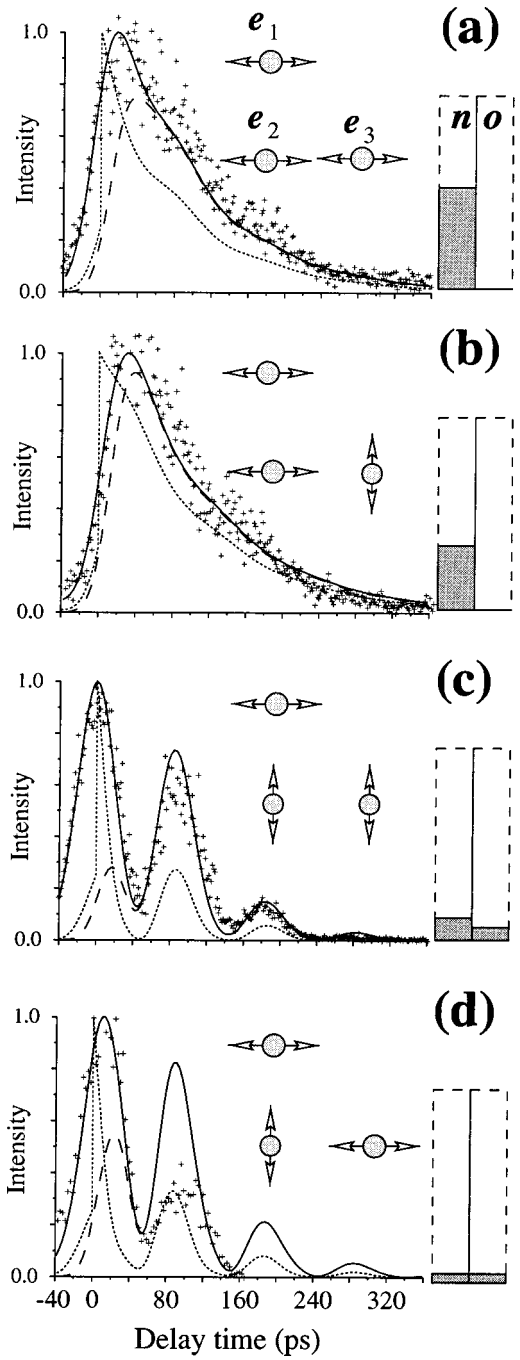

FIG. 6. Experimental DFWM data (crosses) and model calculation (solid line) for the simultaneous excitation of the $Q_1 1$ and $Q_{12} 4$ transitions of OH (see Fig. 5 for explanation of individual curves). Four different polarization configurations of input and output beams are displayed as insets in the upper right portions (a)–(d) of each figure: (a) *XXXX*, (b) *XXYY*, (c) *XYYX*, and (d) *XYXY*. In addition, next to each polarization geometry are depicted the relative amplitudes for the nonoscillating (*n*) and oscillating (*o*) contributions in Eq. (18a), respectively. See text for further explanations.

out to be especially important when multiple transitions of different strengths are excited simultaneously. For our pulse envelopes of $\tau_L \approx 38$ ps full width at half maximum the generated signal is in a transient regime, and the signal intensity will be dependent on the total collision rate. Using simple ideal gas law one calculates 120 ps for the time between gas kinetic collisions of OH and nitrogen in atmospheric pressure gas at 1900 K.

In their DNI calculations Reichard *et al.* [30] found that the inclusion of Doppler broadening, which is the most important molecular contribution to the overall linewidth for the present flame conditions, leads to destructive interference (the different excited velocity groups radiate—with slightly different frequencies—out of phase with each other), which shortens the length of the signal pulse. This was shown to be different for a purely homogeneously broadened line, where the nonlinear polarization—provided collisional dephasing is slow compared to the pulse length—persists in the medium for quite some time after passage of the pump pulses. Consequently, in our experiments the deduced relaxation times as listed in Table II are dominated by rotational energy transfer and population relaxation caused by the environment in both the ground and excited electronic state manifold connected by the exciting laser radiation.

Considering ground- and excited-state populations as well as the polarization properties of angular momentum distributions, DFWM signals can be regarded as arising from contributions of 12 different gratings [34,35]. In addition, in frequency-resolved experiments contributions from thermal gratings can even dominate the DFWM signal at high densities when collisional relaxation and quenching processes take place on a time scale short compared with the temporal pulse length of the signal generating beams [50,51]. This often complicates the interpretation of experimental data obtained in both the frequency and time domains. However, the formation of thermal gratings can be avoided by polarization selection of the incoming beams, and the number of different grating contributions may be reduced by multicolor frequency-resolved experiments [52], or through proper time sequencing in short pulse pump-probe measurements.

The relaxation times determined in the present work (cf. Table II) are in good agreement with our previous results [29,38]. In addition, although slightly larger, they correspond well with fitted relaxation rates of OH in helium diluted hydrogen-oxygen flames deduced from high resolution polarization sensitive DFWM line shape studies in [35]. They estimate an average homogeneous dephasing rate for low ($J=1.5$) and high ($J=8.5$) rotational excitation of OH of 0.047 and 0.038 cm^{-1}, respectively. However, our measurements are only sensitive to contributions from population and orientation relaxation in the multipole expansion. The variation of the rate for alignment relaxation in the fitting algorithm does not have any significant influence on the calculated transients.

VI. CONCLUSIONS

A still unresolved question in a theoretical understanding of frequency as well as time-resolved nonlinear spectroscopic techniques is the relative importance of the various grating types to the overall signal intensity. In the present work the dependence of the DFWM/PS signal intensities on the polarization configuration of the interacting beams was investigated and compared with a detailed theoretical treatment of the signal generation processes in a forward folded box beam phase-matching geometry. A fully quantum-mechanical picture of the light-matter interaction in

DFWM/PS experiments was developed to describe the temporal behavior of the transient signals excited in selected transitions of the OH $A\,^2\Sigma - X\,^2\Pi$ (0,0) electronic band system in atmospheric pressure flames. It was found that in quantum beat experiments a quantitative description of the temporal behavior of the signal intensity rests on three grounds: first, the polarization dependent factors derived from the angular-momentum couplings for each spectroscopic branch excited in the experiment are incorporated into the expression for the signal intensity. Second, if not known accurately enough from experiment adjustment of the peak position and width of the frequency distribution of the interacting laser radiation within experimental uncertainty is appropriate to correctly predict the relative importance of the oscillating and nonoscillating contribution to the temporal signal intensity. Third, it is important to analyze all relevant interaction terms in the perturbative treatment of time ordered energy level diagrams to correctly describe especially the early temporal behavior of the signal trace where all laser pulses are present simultaneously in the sample.

We have calculated the DFWM/PS signal intensity according to Eqs. (A11)–(A13) assuming that both pump and probe beams are coherent. In other words, the frequency spread of the radiation is completely determined by the temporal profile of the laser pulses [see, e.g., Eq. (9)]. However, the laser beams used in the present experiment contain a significant incoherent contribution. This means that their frequency distribution is broad in comparison with the Fourier transform limit of the temporal pulse profile. To describe incoherent scattering terms one has to take into account a complex amplitude factor $E \rightarrow E(\omega)\exp(i\phi)$ for the pump and probe beams [e.g., in Eq. (9)], where ϕ is the phase of the photon mode (ω). The final result has to be averaged over all phases and integrated over all incoherent field modes ω, as was done, e.g., in [33]. This leads to an additional threefold frequency integration in Eq. (A11). In this case a direct numeric integration becomes extremely time consuming and further theoretical analysis is necessary to solve this problem.

For future work, experiments are underway to extend the measurements to other spectral structures of small radicals such as NH in ammonia-oxygen flames, where different collisional environments prevail than in the presently studied methane-air and hydrogen-oxygen flames. The NH $A,\,^3\Pi - X\,^3\Sigma$ triplet electronic band system exhibits dense Q-branch and open R-branch structures, which offers the opportunity to study the gradual change between clearly isolated as well as simultaneous excitation or relaxation phenomena with the short pulse laser system presently available. Furthermore, it is planned to study ground-state relaxation processes through the selective depletion of one populated energy level via a saturating pump beam and a subsequent DFWM-PS probe experiment. This allows a separate study of rotational energy transfer rates in the ground- and excited-state manifolds for molecules in collisionally dominated environments.

ACKNOWLEDGMENTS

The financial support of the Deutsche Forschungsgemeinschaft (Grant No. Dr 195/12) and the Stiftung Volkswagenwerk (Grant No. I/70 491) is gratefully acknowledged. The authors are thankful to J. Wolfrum for his continued interest in this work.

APPENDIX A

Our goal is to represent Eq. (14) in a form that can be directly compared with experimental data. First, we expand the density matrix in this equation over multipole moments (15). Using Eq. (16) one calculates the trace over magnetic quantum numbers in Eq. (14) and obtains

$$
\begin{aligned}
\varepsilon_\alpha = 2\sigma(\pi^2\epsilon_0 c^3 n/\omega^2)^2 \Bigg| \int d\mathbf{v} \int_{-\infty}^{\infty} dx\, \exp[-(x+\omega-\omega_\alpha)^2\sigma/2] \sum_{n'',n_2'} (\mathcal{L}^{(1)}_{n'',n_2'} + i\omega_\alpha - i\mathbf{k}_\alpha\cdot\mathbf{v})^{-1} \\
\times \sum_{n_1'} \sqrt{(2J_1'+1)(2J_2'+1)}\, A^{1/2}_{n_1';n''} A^{1/2}_{n_2';n''} \sum_{K,Q} \Bigg\{ E_3 P(\mathbf{e}_3\cdot\mathbf{e}_\alpha;K,Q)^* \exp[i(x+\omega-\omega_\alpha)\tau] \\
\times \Bigg[(-1)^{2J_2'-J_1'-J''+K} [\mathcal{L}^{(K)}_{n_1';n_2'} - i(\mathbf{k}_\alpha-\mathbf{k}_3)\mathbf{v}+ix]^{-1} \begin{Bmatrix} J'', & J_1', & 1 \\ K, & 1, & J_2' \end{Bmatrix} \\
\times \mathrm{Tr}'\{\exp\{i[\mathbf{k}_\alpha-\mathbf{k}_3(\omega_\alpha-x)]\mathbf{r}\}\tilde{\rho}_1(x)|n_1';n_2';K,Q\rangle\rangle^*\} - (-1)^{J_1'-J''}\delta_{J_2',J_1'}[\mathcal{L}^{(K)}_{n'';n''} - i(\mathbf{k}_\alpha-\mathbf{k}_3)\mathbf{v}+ix]^{-1} \\
\times \begin{Bmatrix} J_1', & J'', & 1 \\ K, & 1, & J'' \end{Bmatrix} \mathrm{Tr}'\{\exp\{i[\mathbf{k}_\alpha-\mathbf{k}_3(\omega_\alpha-x)]\mathbf{r}\}\tilde{\rho}_1(x)|n'';n'';K,Q\rangle\rangle^*\} \Bigg] \\
+ E_1 P(\mathbf{e}_1\cdot\mathbf{e}_\alpha;K,Q)^* \Bigg[(-1)^{2J_2'-J_1'-J''+K} [\mathcal{L}^{(K)}_{n_1';n_2'} - i(\mathbf{k}_\alpha-\mathbf{k}_1)\mathbf{v}+ix]^{-1} \begin{Bmatrix} J'', & J_1', & 1 \\ K, & 1, & J_2' \end{Bmatrix} \\
\times \mathrm{Tr}'\{\exp\{i[\mathbf{k}_\alpha-\mathbf{k}_1(\omega_\alpha-x)]\mathbf{r}\}\tilde{\rho}_3(x)|n_1';n_2';K,Q\rangle\rangle^*\} - (-1)^{J_1'-J''}\delta_{J_2',J_1'}[\mathcal{L}^{(K)}_{n'';n''} - i(\mathbf{k}_\alpha-\mathbf{k}_1)\mathbf{v}+ix]^{-1} \\
\times \begin{Bmatrix} J_1', & J'', & 1 \\ K, & 1, & J'' \end{Bmatrix} \mathrm{Tr}'\{\exp\{i[\mathbf{k}_\alpha-\mathbf{k}_1(\omega_\alpha-x)]\mathbf{r}\}\tilde{\rho}_3(x)|n'';n'';K,Q\rangle\rangle^*\} \Bigg] \Bigg\} \Bigg|^2 ,
\end{aligned}
\tag{A1}
$$

where the prime means that the summation over translational velocities is excluded from the trace. The dependence of the DFWM-PS signal intensity on the polarization configurations of the pump and probe photons is completely described by the polarization factors P in Eq. (17). The matrix elements of the Liouville operator are given in terms of transition frequencies and linewidths determined by the relaxation operator Γ: $\mathcal{L}^{(K)}_{n_1;n_2}=i\omega_{n_1,n_2}+\Gamma^{(K)}_{n_1;n_2}$. Here, advantage is taken of the fact that the relaxation process does not couple multipole moments of different ranks.

We now have to calculate the molecular density matrix distorted by the pump electric field. It is convenient to represent Eq. (12) in the following form:

$$\tilde{\rho}_1(x)=-\frac{1}{\hbar^2}\int_{-\infty}^{\infty}dy\int_0^{\infty}dt\{\tilde{\mathcal{V}}_1(\mathbf{r},x-y)^{\times}\exp[-(\mathcal{L}+iy)t]\tilde{\mathcal{V}}_2^{\dagger}(\mathbf{r},-y)\rho_{\mathrm{eq}}-\tilde{\mathcal{V}}_2^{\dagger}(\mathbf{r},y-x)^{\times}\exp[-(\mathcal{L}+iy)t]\rho_{\mathrm{eq}}\tilde{\mathcal{V}}_1(\mathbf{r},y)\}, \tag{A2}$$

where the Fourier transform of the interaction operator with the pump field is given by

$$\tilde{\mathcal{V}}_n(\mathbf{r},x)=\left(\frac{\sigma}{2\pi}\right)^{1/2}E_n\exp[-i\mathbf{k}_n(x)\mathbf{r}-(x-\omega)^2\sigma/2](\mathbf{d}\cdot\mathbf{e}_n^*). \tag{A3}$$

Substituting Eqs. (A3) into Eq. (A2) one obtains

$$\begin{aligned}\tilde{\rho}_1(x)=\sigma\frac{E_1E_2}{2\pi\hbar^2}\exp[-i(\mathbf{k}_1-\mathbf{k}_2)\cdot\mathbf{r}]\int_{-\infty}^{\infty}dy\int_0^{\infty}dt\exp\{-\sigma[(x-y)^2+y^2]/2-iyt\}\{\exp\{i[\mathbf{k}_2(y-x)-\mathbf{k}_1(y)]\mathbf{r}\}(\mathbf{d}\cdot\mathbf{e}_2)^{\times}\\ \times\exp[-(\mathcal{L}+i\omega-i\mathbf{k}_1\cdot\mathbf{v})t]\rho_{\mathrm{eq}}(\mathbf{d}\cdot\mathbf{e}_1^*)-\exp\{i[\mathbf{k}_1(y-x)-\mathbf{k}_2(y)]\mathbf{r}\}(\mathbf{d}\cdot\mathbf{e}_1^*)^{\times}\exp[-(\mathcal{L}-i\omega+i\mathbf{k}_2\cdot\mathbf{v})t](\mathbf{d}\cdot\mathbf{e}_2)\rho_{\mathrm{eq}}\},\end{aligned} \tag{A4}$$

where the wave vector at the average frequency of the pulse envelope is denoted as $\mathbf{k}\equiv\mathbf{k}(\omega)$. It is assumed that both pump and probe photons are almost collinear. In this case, the dependence on the translational coordinates can be neglected in Eq. (A4). In the present experiments a system with two closely spaced transitions ($n''\rightarrow n_1'$ and $n''\rightarrow n_2'$) in resonance with the external field is considered. Equation (A4) describes the change of the equilibrium population in the ground (n'') and excited (n_1',n_2') levels, which is induced by the interaction with the pump field. Calculating the matrix elements we derive, respectively,

$$\tilde{\rho}_1(x,\mathbf{v})_{n'',n''}=-\frac{\sigma}{2\hbar^2}E_1E_2\exp(-x^2\sigma/4)\sum_{n'}(\mathbf{e}_1^*\cdot\mathbf{d}_{n'',n'})(\mathbf{e}_2\cdot\mathbf{d}_{n',n''})[V_{n',n''}(\omega-x/2;\mathbf{v})+V^*_{n',n''}(\omega+x/2;\mathbf{v})]\rho_{\mathrm{eq}}(n'',\mathbf{v}), \tag{A5a}$$

$$\tilde{\rho}_1(x,\mathbf{v})_{n_1',n_2'}=\frac{\sigma}{2\hbar^2}E_1E_2\exp(-x^2\sigma/4)\sum_{n''}(\mathbf{e}_2\cdot\mathbf{d}_{n_1',n''})(\mathbf{e}_1^*\cdot\mathbf{d}_{n'',n_2'})[V_{n_1',n''}(\omega-x/2;\mathbf{v})+V^*_{n_2',n''}(\omega+x/2;\mathbf{v})]\rho_{\mathrm{eq}}(n'',\mathbf{v}) \tag{A5b}$$

with

$$V_{n',n''}(\omega,\mathbf{v})=V[\sqrt{\sigma}(\mathcal{L}_{n',n''}-i\omega+i\mathbf{k}\cdot\mathbf{v})], \tag{A6}$$

where the Voigt function $V(x)$ can be expressed via the complex error function:

$$V(x)=\exp(x^2)\mathrm{erfc}(x). \tag{A7}$$

The interaction with a second pump and a probe pulse ($\tilde{\rho}_3$) given by Eq. (13) can be calculated in the same manner. However, this procedure leads to a rather complex functional dependence on the delay time (τ) between pump and probe pulses. In contrast, the time decay in case I is determined by a simple Fourier transformation in Eq. (A1). In other words, the entire kinetics can be obtained by a single integration over frequencies (using the fast Fourier transform algorithm). The kinetics in case II also can be written in terms of the Fourier transformation if we change the order of integration in Eqs. (13) and (14). After some algebra one arrives at the following result:

$$\int_{-\infty}^{\infty} dx \exp[-(x+\omega-\omega_\alpha)^2\sigma/2][(\mathcal{L}+ix)^{-1}\tilde{\rho}_3(x)]_{n_1,n_2}$$

$$= \int_{-\infty}^{\infty} dx \exp[-(x+\omega-\omega_\alpha)^2\sigma/2 + i(x+\omega-\omega_\alpha)\tau] V_{n_1,n_2}(\omega-\omega_\alpha+x/2;0)\tilde{\rho}_3^{(1)}(x,\mathbf{v})_{n_1,n_2}$$

$$+ \sum_n [V_{n_1,n_2}(\omega-\omega_\alpha+x/2;0) - V_{n_1,n}(\omega-x/2;\mathbf{v})]\tilde{\rho}_3^{(2)}(x,\mathbf{v})_{n_1,n_2;n}, \tag{A8}$$

where $\tilde{\rho}_3^{(1)}$ determines the contribution to the DFWM signal when the scattering of the probe photon precedes the interaction of both pump photons with the molecule. The transformation of the density matrix in this case is given for the ground and excited states, respectively, as

$$\tilde{\rho}_3^{(1)}(x,\mathbf{v})_{n'',n''} = -\frac{\sigma}{2\hbar^2} E_3 E_2 \exp(-x^2\sigma/4) \sum_{n'} (\mathbf{e}_3^* \mathbf{d}_{n'',n'})(\mathbf{e}_2 \mathbf{d}_{n',n''})(\mathcal{L}_{n'',n'} + i\omega_\alpha - ix - i\mathbf{k}\mathbf{v})^{-1} \rho_{\mathrm{eq}}(n'',\mathbf{v}), \tag{A9a}$$

$$\tilde{\rho}_3^{(1)}(x,\mathbf{v})_{n_1',n_2'} = \frac{\sigma}{2\hbar^2} E_3 E_2 \exp(-x^2\sigma/4) \sum_{n''} (\mathbf{e}_2 \cdot \mathbf{d}_{n_1',n''})(\mathbf{e}_3^* \cdot \mathbf{d}_{n'',n_2'})(\mathcal{L}_{n'',n_2'} + i\omega_\alpha - ix - i\mathbf{k}\cdot\mathbf{v})^{-1} \rho_{\mathrm{eq}}(n'',\mathbf{v}). \tag{A9b}$$

Similarly, $\tilde{\rho}^{(2)}$ describes the scattering signal when the probe photon arrives between the pump photons in the interaction region. In this case, due to the preceding interaction with the pump photon (p_2) the density matrix is off diagonal. This intermediate state is of importance in the last sum in Eq. (A8) and is labeled by the third additional index. For the matrix elements in the ground and excited states one has, respectively,

$$\tilde{\rho}_3^{(2)}(x,\mathbf{v})_{n'',n'';n'} = -\frac{\sigma}{2\hbar^2} E_3 E_2 \exp(-x^2\sigma/4)(\mathbf{e}_3^* \cdot \mathbf{d}_{n'',n'})(\mathbf{e}_2 \cdot \mathbf{d}_{n',n''})(\mathcal{L}_{n',n''} - \mathcal{L}_{n'',n''} - i\omega_\alpha + ix + i\mathbf{k}\cdot\mathbf{v})^{-1} \rho_{\mathrm{eq}}(n'',\mathbf{v}), \tag{A10a}$$

$$\tilde{\rho}_3^{(2)}(x,\mathbf{v})_{n_1',n_2';n''} = \frac{\sigma}{2\hbar^2} E_3 E_2 \exp(-x^2\sigma/4)(\mathbf{e}_2 \cdot \mathbf{d}_{n_1',n''})(\mathbf{e}_3^* \cdot \mathbf{d}_{n'',n_2'})(\mathcal{L}_{n_1',n''} - \mathcal{L}_{n_1',n_2'} - i\omega_\alpha + ix + i\mathbf{k}\cdot\mathbf{v})^{-1} \rho_{\mathrm{eq}}(n'',\mathbf{v}). \tag{A10b}$$

Expanding the distributions (A5), (A9), and (A10) in terms of the multipole moments and using them in Eq. (A1) we derive the final result for the energy density of the DFWM signal:

$$\varepsilon_\alpha = \zeta(T) n^2 \sigma^3 E_1^2 E_2^2 E_3^2 \left| \int_{-\infty}^{\infty} dx \exp\{-\sigma[(x+\omega-\omega_\alpha)^2/2 + x^2/4] + ix\tau\} \right.$$

$$\left. \times \int_{-\infty}^{\infty} dv \sum_{n_1',n_2'} \frac{\exp(-mv^2/2k_BT)}{\mathcal{L}^{(1)}_{n'',n_2'} + i\omega_\alpha - ikv} A_{n_1';n''} A_{n_2';n''} (2J_1'+1)(2J_2'+1) \sum_K \{\mathcal{S}_1(n_1',n_2',n'';K) + \mathcal{S}_3(n_1',n_2',n'';K)\} \right|^2, \tag{A11}$$

where the subscript (K) defines the multipole rank of the Liouville operator in Eq. (A7). The temperature dependence of $\zeta(T)$ is determined by the Boltzmann population distribution within the ground level

$$\zeta(T) = \frac{\pi m}{kT} \left[\frac{\pi^2 c^6 \epsilon_0^2}{2\hbar\omega^5 Q(T)} \exp\left(-\frac{E_{n''}}{k_B T} \right) \right]^2, \tag{A12}$$

with the partition function $Q(T)$. The contributions to the DFWM signal provided by the scattering processes in cases I and II are denoted as $\mathcal{S}_1$ and $\mathcal{S}_3$, respectively:

$$\mathcal{S}_1(n_1',n_2',n'';K) = \sum_Q P(\mathbf{e}_3,\mathbf{e}_\alpha;K,Q)^* P(\mathbf{e}_2,\mathbf{e}_1;K,Q) \left[\begin{Bmatrix} J_1', & J'', & 1 \\ K, & 1, & J'' \end{Bmatrix} \begin{Bmatrix} J_2', & J'', & 1 \\ K, & 1, & J'' \end{Bmatrix} \right.$$

$$\times (-1)^{J_1'+J_2'} (\mathcal{L}^{(K)}_{n'',n''} + ix)^{-1} [V_{n_1',n''}(\omega - x/2;v) + V^*_{n_1',n''}(\omega + x/2;v)]$$

$$\left. + (-1)^{2J_1'} \begin{Bmatrix} J'', & J_1', & 1 \\ K, & 1, & J_2' \end{Bmatrix}^2 (\mathcal{L}^{(K)}_{n_1',n_2'} + ix)^{-1} [V_{n_1',n''}(\omega - x/2;v) + V^*_{n_2',n''}(\omega + x/2;v)] \right], \tag{A13a}$$

$$\mathcal{S}_3(n_1',n_2',n'';K)=\sum_Q P(\mathbf{e}_1,\mathbf{e}_\alpha;K,Q)^*P(\mathbf{e}_2,\mathbf{e}_3;K,Q)\left[\begin{Bmatrix} J_1', & J'', & 1 \\ K, & 1, & J'' \end{Bmatrix}\begin{Bmatrix} J_2', & J'', & 1 \\ K, & 1, & J'' \end{Bmatrix}\right.$$
$$\times(-1)^{J_1'+J_2'}\{V^{(K)}_{n'',n''}(\omega-\omega_\alpha+x/2;0)(\mathcal{L}^{(1)}_{n'',n_1'}+i\omega_\alpha-ix-ikv)^{-1}$$
$$+[V^{(K)}_{n'',n''}(\omega-\omega_\alpha+x/2;0)-V^{(1)}_{n'',n_1'}(\omega-x/2;v)](\mathcal{L}^{(1)}_{n_1',n''}-\mathcal{L}^{(K)}_{n'',n''}-i\omega_\alpha+ix+ikv)^{-1}\}$$
$$+(-1)^{2J_1'}\begin{Bmatrix} J'', & J_1', & 1 \\ K, & 1, & J_2' \end{Bmatrix}^2\{V^{(K)}_{n_1',n_2'}(\omega-\omega_\alpha+x/2;0)(\mathcal{L}^{(1)}_{n'',n_2'}+i\omega_\alpha-ix-ikv)^{-1}$$
$$\left.+[V^{(K)}_{n_1',n_2'}(\omega-\omega_\alpha+x/2;0)-V^{(1)}_{n_1',n''}(\omega-x/2;v)](\mathcal{L}^{(1)}_{n_1',n''}-\mathcal{L}^{(K)}_{n_1',n_2'}-i\omega_\alpha+ix+ikv)^{-1}\}\right]. \quad \text{(A13b)}$$

[1] S. Kinoshita, Y. Kai, M. Yamaguchi, and T. Yagi, Chem. Phys. Lett. **236**, 259 (1995).
[2] S. Mukamel, *Principles of Nonlinear Optical Spectroscopy* (Oxford University Press, New York, 1995).
[3] S. Haroche, Top. Appl. Phys. **13**, 252 (1976).
[4] H. Bitto and J. R. Huber, Acc. Chem. Res. **25**, 65 (1992).
[5] E. F. McCormack, S. T. Pratt, P. M. Dehmer, and J. L. Dehmer, Chem. Phys. Lett. **227**, 656 (1994).
[6] A. C. Eckbreth, *Laser Diagnostics for Combustion Temperature and Species*, Combustion Science and Technology Vol. 3 (Gordon and Breach, Amsterdam, 1996).
[7] K. Kohse Höinghaus, Prog. Energy Combust. Sci. **20**, 203 (1994).
[8] R. L. Abrams and R. C. Lind, Opt. Lett. **2**, 94 (1978).
[9] *Optical Phase Conjugation*, edited by R. A. Fisher (Academic, New York, 1983).
[10] R. E. Teets, F. W. Kowalski, W. T. Hill, N. Charlson, and T. W. Hänsch, Proc. Soc. Photo-Opt. Instrum. Eng. **113**, 80 (1977).
[11] W. Demtröder, *Laser Spectroscopy* (Springer-Verlag, Berlin, 1993).
[12] J. T. Fourkas, R. Trebino, and M. D. Fayer, J. Chem. Phys. **97**, 69 (1992).
[13] P. Ewart and S. V. O'Leary, Opt. Lett. **11**, 279 (1986).
[14] T. Dreier and D. J. Rakestraw, Opt. Lett. **15**, 72 (1990).
[15] K. Nyholm, R. Maier, C. G. Aminoff, and M. Kaivola, Appl. Opt. **32**, 919 (1993).
[16] D. S. Green, T. G. Owano, S. Williams, D. G. Goodwin, R. N. Zare, and C. H. Kruger, Science **259**, 1726 (1993).
[17] Y. Tang and S. A. Reid, Chem. Phys. Lett. **248**, 476 (1996).
[18] G. J. Germann, A. McIlroy, T. Dreier, R. L. Farrow, and D. J. Rakestraw, Ber. Bunsenges. Phys. Chem. **97**, 1630 (1993).
[19] T. Dreier and D. Rakestraw, Appl. Phys. B: Photophys. Laser Chem. **50**, 479 (1990).
[20] S. J. Tsay, K. G. Owens, K. W. Aniolek, D. L. Miller, and N. P. Cernansky, Opt. Lett. **20**, 1725 (1995).
[21] K. Nyholm, K. Kaivola, and C. G. Aminoff, Appl. Phys. B: Photophys. Laser Chem. **60**, 5 (1995).
[22] R. L. Farrow, D. J. Rakestraw, and T. Dreier, J. Opt. Soc. Am. B **9**, 1770 (1992).
[23] H. Graener, G. Seifert, and A. Laubereau, Chem. Phys. Lett. **172**, 435 (1990).
[24] K. Iwata, W. L. Weaver, and T. L. Gustafson, Chem. Phys. Lett. **210**, 50 (1993).
[25] M. Morgen, W. Price, L. Hunziker, P. Ludowise, M. Blackwell, and Y. Chen, Chem. Phys. Lett. **209**, 1 (1993).
[26] S. A. Akhmanov, N. I. Koroteev, S. A. Magnitskii, V. B. Morozov, A. P. Tarasevich, and V. G. Tunkin, J. Opt. Soc. Am. B **2**, 640 (1985).
[27] W. Schade, J. Walewski, A. Offt, and A. Knaak, Phys. Rev. A **53**, R2921 (1996).
[28] A. Dreizler, R. Tadday, A. A. Suvernev, M. Himmelhaus, T. Dreier, and P. Foggi, Chem. Phys. Lett. **240**, 315 (1995).
[29] R. Tadday, A. Dreizler, A. A. Suvernev, and T. Dreier, J. Mol. Struct. **410-411**, 85 (1997).
[30] T. A. Reichardt and R. P. Lucht, J. Opt. Soc. Am. B **13**, 2807 (1996).
[31] J. G. Fujimoto and T. K. Yee, IEEE J. Quantum Electron. **19**, 861 (1983).
[32] J. G. Fujimoto and T. K. Yee, IEEE J. Quantum Electron. **22**, 1215 (1986).
[33] J. Cooper, A. Charlton, D. R. Meacher, P. Ewart, and G. Alber, Phys. Rev. A **40**, 5705 (1989).
[34] S. Williams, R. N. Zare, and L. A. Rahn, J. Chem. Phys. **101**, 1072 (1994).
[35] S. Williams, L. A. Rahn, and R. N. Zare, J. Chem. Phys. **104**, 3947 (1996).
[36] H. Li and W. Kong, J. Chem. Phys. **107**, 3774 (1997).
[37] M. Schmitt, G. Knopp, A. Materny, and W. Kiefer, Chem. Phys. Lett. **280**, 339 (1997).
[38] R. Tadday, A. A. Suvernev, T. Dreier, and J. Wolfrum, Chem. Phys. Lett. **268**, 117 (1997).
[39] J. Ö. Bjarnason, B. S. Hudson, and H. C. Andersen, J. Chem. Phys. **70**, 4130 (1979).
[40] S. Mukamel and E. Hanamura, Phys. Rev. A **33**, 1099 (1986).
[41] A. A. Suvernev, Phys. Rev. A **50**, 107 (1994).
[42] A. Ben-Reuven, Phys. Rev. **145**, 7 (1966).
[43] R. C. Hilborn, Am. J. Phys. **50**, 982 (1982).
[44] R. J. Abraham, *Introduction to Nuclear Magnetic Resonance Spectroscopy* (Wiley, New York, 1988).
[45] M. S. Brown, L. A. Rahn, and T. Dreier, Opt. Lett. **17**, 76 (1992).
[46] S. Williams, R. N. Zare, and L. A. Rahn, J. Chem. Phys. **101**, 1093 (1994).

[47] A. Lawitzki, I. Plath, W. Stricker, J. Bittner, U. Meier, and K. Kohse-Höinghaus, Appl. Phys. B: Photophys. Laser Chem. **50**, 513 (1990).

[48] J. E. M. Goldsmith, in *Proceedings of the 20th International Symposium on Combustion* (The Combustion Institute, Pittsburgh, 1984), p. 1331.

[49] J. Luque and D. R. Crosley, SRI International Report No. MP 96-001 (1996).

[50] S. Williams, R. A. Rahn, P. H. Paul, J. W. Forsman, and R. N. Zare, Opt. Lett. **19**, 1681 (1994).

[51] A. Dreizler, T. Dreier, and J. Wolfrum, Chem. Phys. Lett. **233**, 525 (1995).

[52] W.-C. Hung, M.-L. Huang, Yu.-C. Lee, and Yu.-P. Lee, J. Chem. Phys. **103**, 9941 (1995).